

Gas infall in the massive star formation core G192.16-3.84

Mengyao Tang¹, Sheng-Li Qin¹, Tie Liu^{2,3} and Yuefang Wu⁴

¹ Department of Astronomy, Yunnan University, and Key Laboratory of Astroparticle Physics of Yunnan Province, Kunming, 650091, China, mengyao_tang@yeah.net, slqin@bao.ac.cn

² Korea Astronomy and Space Science Institute, 776 Daedeokdaero, Yuseong-gu, Daejeon 34055, Republic of Korea, liu@kasi.re.kr

³ East Asian Observatory, 660 N. A'ohoku Place, Hilo, HI 96720, USA

⁴ Department of Astronomy, Peking University, 100871, Beijing China, ywu@pku.edu.cn

Received 20xx month day; accepted 20xx month day

Abstract Previous observations have revealed an accretion disk and outflow motion in high-mass star-forming region G192.16-3.84. While collapse have not been reported before. We present here molecular line and continuum observations toward massive core G192.16-3.84 with the Submillimeter Array. C¹⁸O(2-1) and HCO⁺(3-2) lines show pronounced blue profiles, indicating gas infalling in this region. This is the first time that the infall motion has been reported in G192.16-3.84 core. Two-layer model fitting gave infall velocities of 2.0 ± 0.2 and 2.8 ± 0.1 km s⁻¹. Assuming that the cloud core follows a power-law density profile ($\rho \propto r^{1.5}$), the corresponding mass infall rates are $(4.7 \pm 1.7) \times 10^{-3}$ and $(6.6 \pm 2.1) \times 10^{-3} M_{\odot} \text{ yr}^{-1}$ for C¹⁸O(2-1) and HCO⁺(3-2), respectively. The derived infall rates are in agreement with the turbulent core model and those in other high-mass star-forming regions, suggesting that high accretion rate is a general requirement to form a massive star.

Key words: ISM: individual objects (G192.16-3.84) — ISM: molecules — stars: formation

1 INTRODUCTION

Current observational evidences suggest that the low-mass star formation typically starts with a collapsing core inside a molecular cloud. Then, the protostellar objects increase their mass by gas accretion. Meanwhile, it is also accompanied by outflows and accretion disk. Collapse, accretion disk and outflow, therefore, are key elements in low mass star formation. However, the physical conditions and dynamical processes of high-mass star formation are still not well understood, due to observational difficulties caused by their short lifetimes and large distances. Outflows are often found in the high-mass star-forming regions (Wu et al. 2004; Qin et al. 2008; Qiu et al. 2012). Only a handful of disks in high-mass young stellar objects, however, have been detected (Zhang et al. 1998; Shepherd, Claussen & Kurtz 2001; Jiang et al. 2005; Patel

G192.16-3.84 (hereafter G192.16) is a massive protostellar system located at a distance of 1.52 ± 0.08 kpc (Shiozaki et al. 2011). The luminosity of $\sim 3 \times 10^3 L_{\odot}$ implies the presence of an early B star with a mass of 8 to $10 M_{\odot}$ in this region (Shepherd & Churchwell 1996; Shepherd et al. 1998). Rich H_2O masers (Shepherd et al. 2004; Imai et al. 2006; Shiozaki et al. 2011), UC H_{II} region (Hughes & MacLeod 1993; Shepherd & Kurtz 1999), bipolar CO outflows (Shepherd et al. 1998; Liu et al. 2013), rotational motions (Liu et al. 2013) and a solar system-size accretion disk (Shepherd, Claussen & Kurtz 2001) have been observed in G192.16 region, suggesting that massive star is forming in this region. However, collapse of G192.16 core has not been reported before.

In this paper, we present Submillimeter Array (SMA)¹ observations of 230 GHz, 265 GHz, 345 GHz band data towards G192.16, showing collapsing motions in this region.

2 DATA

All observational data used in our work are taken from the Submillimeter Array (SMA) archive. The 230 GHz, 265 GHz, and 345 GHz observations were performed with SMA in August 2005, December 2006, and December 2011, respectively. The 230 GHz data cover CO(2-1), $^{13}CO(2-1)$, $C^{18}O(2-1)$, and SO(6₅-5₄) lines with an uniform spectral resolution of 0.8125 MHz. $HCO^+(3-2)$ and HCN(3-2) transitions were observed in 265 GHz band with hybrid high-spectral resolution. The 265 GHz data have different spectral resolutions in different windows. We resample the 265 GHz band data to uniform resolution of 0.8125 MHz. The 345 GHz data have spectral resolution of 0.8125 MHz and include CO(3-2) and SO(8₈-7₇) lines. Other observational informations such as phase tracking center, bandpass calibrators, gain calibrators, and flux calibrators are listed in Table 1. Data reduction and imaging were made in MIRIAD (Sault et al. 1995). The continuum images were made from line free channels. Self-calibration on the continuum data were made to remove residual errors, and then the gain solutions were applied to line data. The synthesized beam sizes of continuum are summarized in Table 1.

Table 1: SMA Observations

Phase Tracking Center (R.A, Decl.)	Band	N_{ant}^a	Calibrator			Beam Size '' \times ''($^{\circ}$)
			Bandpass	Gain	Flux	
(5 ^h 58 ^m 13 ^s .899, 16 $^{\circ}$ 31'59''.997)	230 GHz	8	3C454.3	0530+135,0510+180	Uranus	3.74'' \times 3.04''(-86 $^{\circ}$)
(5 ^h 58 ^m 13 ^s .530, 16 $^{\circ}$ 31'58''.300)	265 GHz	8	3C273	0528+134,0507+179	Titan	0.86'' \times 0.86''(85 $^{\circ}$)
(5 ^h 58 ^m 13 ^s .549, 16 $^{\circ}$ 31'58''.300)	345 GHz	8	3C84,Uranus	0530+135,0730-116	Titan	1.80'' \times 1.59''(-58 $^{\circ}$)

^a Number of Antennas

¹ The Submillimeter Array is a joint project between the Smithsonian Astrophysical Observatory and the Academia Sinica Institute

3 RESULTS

3.1 Continuum

Figure 1 presents the continuum flux density maps in both color-scale and contours. From Figure 1, one can see that the continuum images at the three wavebands show compact source structure and are unresolved.

Two dimension (2D) Gaussian fitting was made to the compact core. The peak position of the continuum is R.A.(J2000) = $5^h 58^m 13^s .547$, Decl.(J2000) = $16^\circ 31' 58''.206$, which is consistent with that of previous continuum observations and UC H_{II} region (Shepherd et al. 1998; Shepherd & Kurtz 1999; Shepherd, Claussen & Kurtz 2001; Shiozaki et al. 2011; Liu et al. 2013). The deconvolved size, peak flux density, total flux from Gaussian fitting are given in Table 2.

Continuum at our observed wavebands contains free-free emission ($S_\nu \propto \nu^{-0.1}$). Based on measured total flux of 1.5 mJy at the 3.6 cm band (Shepherd & Kurtz 1999), we estimate that the free-free continuum emission are 1.07 mJy and 1.03 mJy at the 230 GHz and 345 GHz bands. Comparing with total flux of the continuum at 230 and 345 GHz (0.270 to 0.769 Jy), the free-free continuum emission is negligible.

To derive physical parameters, we performed spectral energy distribution (SED) fitting based on the data from our observations and the previous data at different wavelengths (Beuther et al. 2002; Shepherd et al. 1998; Shepherd, Claussen & Kurtz 2001; Williams et al. 2004). Figure 2 shows a plot of spectral energy distribution. The best SED fitting gave dust temperature T_d of 71.7 ± 0.4 K, H₂ gas column density N_{H_2} of $(2.7 \pm 1.2) \times 10^{24} \text{ cm}^{-2}$, and dust emissivity index (β) of 1.7 ± 0.4 . Derived dust temperature $T_d = 71.7 \pm 0.4$ K is well consistent with SO₂ rotation temperature $T_{rot}^{SO_2} \sim 84_{-15}^{+18}$ K reported by Liu et al. (2013), indicating that gas is well coupled with dust.

Gas mass of G192.16 continuum core can be calculated by below formula:

$$M_{H_2} = \pi R^2 \cdot m_H \cdot \mu \cdot N_{H_2}, \quad (1)$$

where $\mu = 2.8$ is mean molecular weight (Kauffmann et al. 2008), m_H is mass of H atom. $R = \sqrt{ab}D$ is source size, major and minor axes (a and b) are obtained from 2D Gaussian fitting toward continuum core (as listed in Table 2). Note that we take major and minor axes (a and b) as $1.3''$ and $0.7''$, which are averaged values of 2D Gaussian fitting results of all continuum sources. At a distance of 1.52 kpc, the core radius is calculated as $R = 0.007$ pc. Core mass (M_{H_2}) is derived to be $10.8 \pm 4.8 M_\odot$, which is consistent with the mass range of $4 M_\odot \leq M_{\text{gas}} + M_{\text{dust}} \leq 18 M_\odot$ estimated by Shiozaki et al. (2011).

Table 2: Parameters of Continuum Images

Frequency	Deconvolved Size	Peak Flux Density	Total Flux	RMS
GHz	$a'' \times b''$ (P.A.°)	Jy beam ⁻¹	Jy	Jy beam ⁻¹
230.538 GHz	$1.5'' \times 0.7''$ (121°)	0.239 ± 0.003	0.270 ± 0.003	0.001
265.895 GHz	$0.9'' \times 0.6''$ (179°)	0.170 ± 0.004	0.377 ± 0.008	0.002
345.796 GHz	$1.6'' \times 0.8''$ (146°)	0.511 ± 0.017	0.769 ± 0.029	0.004

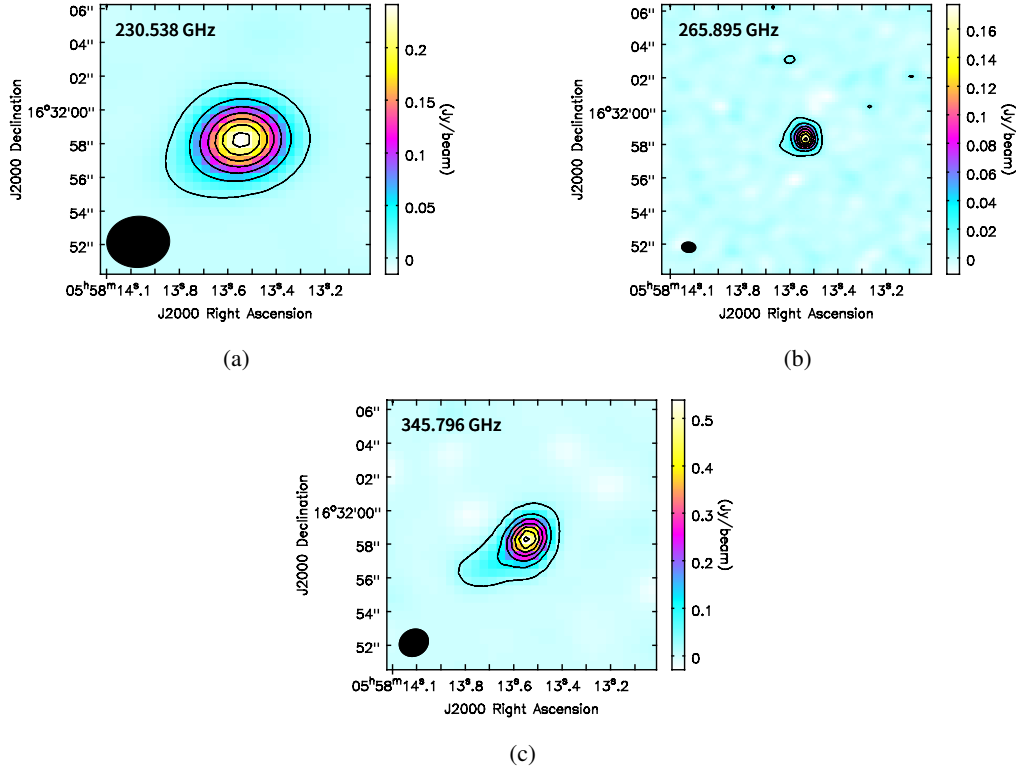


Fig. 1: Panels (a), (b), and (c) present continuum images of 230.538, 265.895, and 345.896 GHz, respectively. For all panels, the contours are from 5% to 95% of peak values (peak values are shown in Table 2), with a step of 15%. The synthesized beam size is shown in bottom-left corner of each panel.

3.2 Molecular lines

Molecular transitions of CO(3-2), CO(2-1), $^{13}\text{CO}(2-1)$, $\text{C}^{18}\text{O}(2-1)$, HCN(3-2), $\text{HCO}^+(3-2)$, $\text{SO}(8_8-7_7)$, and $\text{SO}(6_5-5_4)$ are detected as shown in Figure 3. In Figure 3, CO(3-2), CO(2-1), $^{13}\text{CO}(2-1)$, $\text{C}^{18}\text{O}(2-1)$, HCN(3-2), and $\text{HCO}^+(3-2)$ spectra show double-peaked line profiles with absorption dips at around $\sim 6 \text{ km s}^{-1}$, and the blue-shifted peaks are stronger than red-shifted ones. While $\text{SO}(8_8-7_7)$ and $\text{SO}(6_5-5_4)$ lines show single peak profiles with LSR velocities at $\sim 6 \text{ km s}^{-1}$. These double-peaked spectral profiles are so-called “blue profile” (Zhou et al. 1993; Wu & Evens 2003; Wu et al. 2007), indicating gas infall in this region.

Various molecular tracers (CO, CN, HCN, H_2CO , HCO^+ , and etc.) are used for identifying collapse candidates and studying infall (Fuller, Williams, & Sridharan 2002; Zapata et al. 2008; Wu et al. 2009, 2014; Liu et al. 2011a,b, 2013a,b; Pineda et al. 2012; Qin et al. 2016; Qiu et al. 2012). Simulations by Smith et al. (2012, 2013) suggested that HCN(3-2) and $\text{HCO}^+(3-2)$ are best ones for studying gas infall. From Figure 3, CO(3-2), CO(2-1), $^{13}\text{CO}(2-1)$ and HCN(3-2) lines reveal much wider line wings, and these line wings may be produced by outflow motions (Shepherd et al. 1998; Liu et al. 2013). Therefore, infall “profile” of these lines will be contaminated by outflows. $\text{C}^{18}\text{O}(2-1)$ and $\text{HCO}^+(3-2)$ lines without obvious line wings will be used for further analyses. Note that observations of $\text{C}^{18}\text{O}(2-1)$ and $\text{HCO}^+(3-2)$ lines have

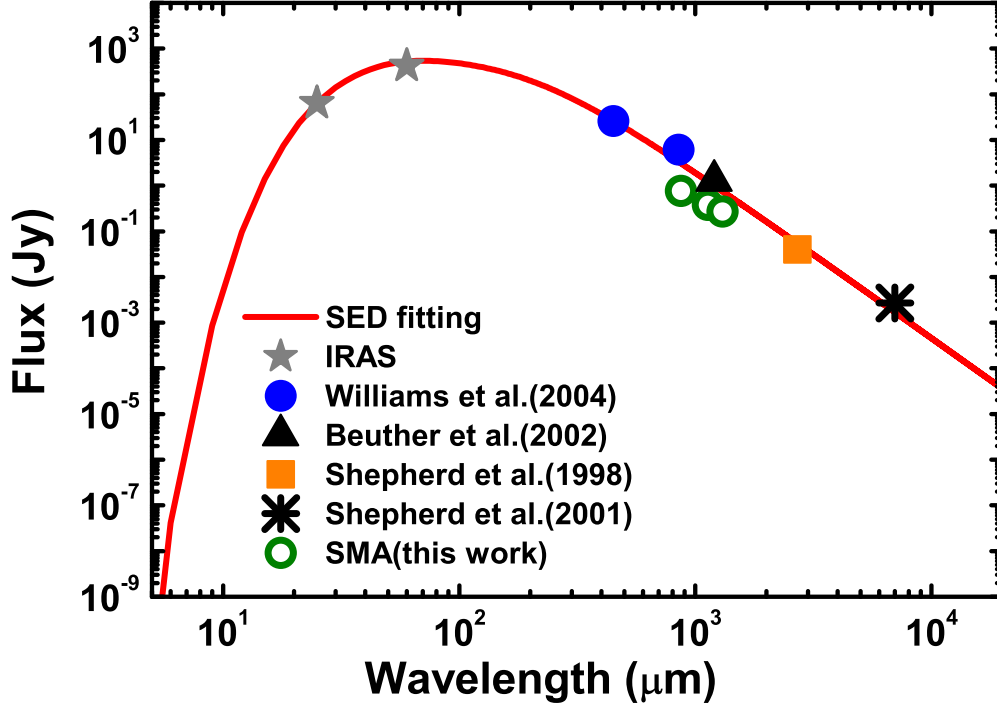


Fig. 2: Spectral energy distribution (SED) fitting obtained from our SMA images complemented with literature and archival data at wavelengths ranging from 25 μm to 7 mm. Red line represents best SED fitting. The data points are shown in gray stars (*IRAS*: 25 μm and 60 μm), blue dots ([Williams et al. 2004](#)), black triangle ([Beuther et al. 2002](#)), orange square ([Shepherd et al. 1998](#)), black asterisk ([Shepherd, Claussen & Kurtz 2001](#)), and green open circles (this work).

The integrated intensity maps of $\text{C}^{18}\text{O}(2-1)$ and $\text{HCO}^+(3-2)$ are presented in Figure 4. The red cross of each panel represents the continuum emission peak. For $\text{C}^{18}\text{O}(2-1)$ map, one can see that the gas emission peak is associated with the continuum peak position. However, the $\text{HCO}^+(3-2)$ gas is separated to two components, and one of them is also associated with continuum peak position.

For collapsing cloud, in case that brightness temperature of the background continuum is brighter than excitation temperature of “blue profile” line transition tracing infall motion, the “blue profile” line will be becoming “inverse P-Cygni” profile. The modified two-layer model ([Myers et al. 1996](#); [Di Francesco et al. 2001](#)) can fit both “blue profile” and “inverse P-Cygni” profile, but also “red profile” and “P-Cygni” profile characterizing of outflows or expansion. Then the modified two-layer model ([Myers et al. 1996](#); [Di Francesco et al. 2001](#)) is adopted to fit spectral profiles of $\text{C}^{18}\text{O}(2-1)$ and $\text{HCO}^+(3-2)$. The panels (a) and (b) of Figure 5 show observed spectra in black and two-layer modelling in red for $\text{C}^{18}\text{O}(2-1)$ and $\text{HCO}^+(3-2)$, respectively. The two-layer model can be simply described as follow:

$$\Delta T_B = (J_f - J_{cr})[1 - e^{(-\tau_f)}] + (1 - \Phi)(J_r - J_b)[1 - e^{(-\tau_r - \tau_f)}], \quad (2)$$

where

$$J_{cr} = \Phi J_c + (1 - \Phi)J_r, \quad (3)$$

$$\tau_r = \tau_0 e^{\left[\frac{-(V+V_{\text{in}}-V_{\text{LSR}})^2}{2\sigma^2}\right]}. \quad (5)$$

The model takes optical depth (τ_0), front layer radiation temperature (J_f), rear layer radiation temperature (J_r), LSR velocity (V_{LSR}), velocity dispersion (σ), infall velocity (V_{in}), radiation temperatures of the continuum source (J_c) and fill factor (Φ) into account. We adopted dust temperature $T_d = 71.7$ K from our SED fitting as radiation temperature (J_c) of continuum source, and the fill factor (Φ) is fixed to 0.3 during the fitting process. The similar procedure was also used by [Pineda et al. \(2012\)](#). The V_{LSR} is fixed to 6 km s^{-1} , which is derived by SO(6₅-5₄) line. During the fitting process, only τ_0 , J_f , J_r , σ , and V_{in} are free parameters, the parameter spaces are 0.1~10 for τ_0 , 3~100 K for J_f and J_r , 0.1~10 km s^{-1} for V_{in} . The Levenberg-Marquardt (L-M) algorithm was adopted to search for best solution.

The best fitting gave infall velocities of C¹⁸O(2-1) and HCO⁺(3-2) spectra are 2.0 ± 0.2 and 2.8 ± 0.1 km s^{-1} , respectively. The detailed fitting results are presented in Table 3. We find that τ_0 , J_f , and J_r are interdependent and very sensitive to initial values. Thus, they can not be determined accurately. In contrast, σ and V_{in} mainly determine the line profile. Thus, they are much less sensitive to initial values and more reliable.

Assuming that the cloud has a power-law density profile ($\rho \propto r^{-1.5}$), the mass enclosed in r_0 can be calculated by ([Liu et al. 2018](#))

$$M = \int_0^{r_0} 4\pi r^2 \rho_0 \left(\frac{r}{r_0}\right)^{-1.5} dr, \quad (6)$$

where r_0 is the outer radius and ρ_0 is the density at r_0 . Thus, the mass infall rate can be estimated as

$$M_{\text{in}} = 4\pi r_0^2 \rho_0 V_{\text{in}} = 1.5 M V_{\text{in}} / r_0. \quad (7)$$

We adopt the mass of $10.8 M_{\odot}$ from SED fitting for M , and averaged source size (R) 0.007 pc for r_0 . Thus the mass infall rates of C¹⁸O(2-1) and HCO⁺(3-2) are estimated to be $(4.7 \pm 1.7) \times 10^{-3}$ and $(6.6 \pm 2.1) \times 10^{-3} M_{\odot} \text{ yr}^{-1}$, respectively. The infall rates are also summarized in Table 3.

Table 3: The Fitting Results of Two-layer Model

Line	τ_0	J_f (K)	J_r (K)	σ (km s^{-1})	V_{in} (km s^{-1})	M_{in} $M_{\odot} \text{ yr}^{-1}$
C ¹⁸ O(2-1)	0.7 ± 0.4	23.8 ± 2.4	11.1 ± 4.7	0.9 ± 0.4	2.0 ± 0.2	$(4.7 \pm 1.7) \times 10^{-3}$
HCO ⁺ (3-2)	0.4 ± 0.1	23.6 ± 0.3	5.5 ± 0.4	1.4 ± 0.1	2.8 ± 0.1	$(6.6 \pm 2.1) \times 10^{-3}$

Notes: Optically depth (τ_0), front layer radiation temperature (J_f), rear layer radiation temperature (J_r), LSR velocity (V_{LSR}), velocity dispersion (σ), infall velocity (V_{in}) are free parameters in fitting, while infall rate (M_{in}) is calculated by using fitted infall velocity.

4 DISCUSSION AND CONCLUSION

Rich H₂O masers ([Shepherd et al. 2004](#); [Imai et al. 2006](#); [Shiozaki et al. 2011](#)), UC H_{II} region ([Hughes & MacLeod 1993](#); [Shepherd & Kurtz 1999](#)), bipolar CO(1-0) outflows ([Shepherd et al. 1998](#); [Liu et al. 2013](#)), and an accretion disk ([Shepherd, Claussen & Kurtz 2001](#)) in G192.16 have been reported by previous

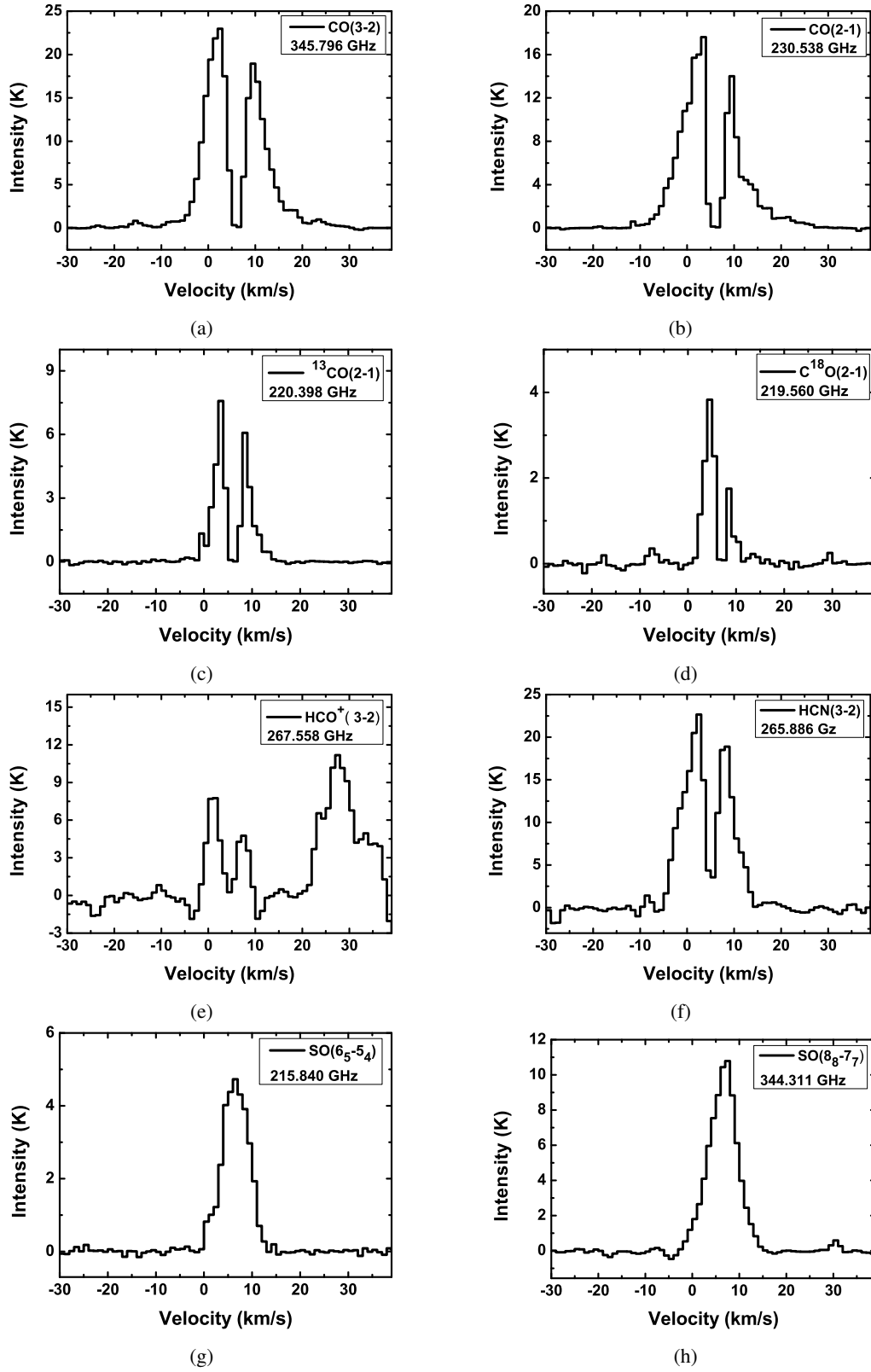


Fig. 3: All spectra are extracted from continuum emission peak position. Line name and rest frequency are shown in upper-right corner of each panel.

We have identified gas infall in G192.16 region using $\text{C}^{18}\text{O}(2-1)$ and $\text{HCO}^+(3-2)$ lines, for the first time. The infall rates derived from these transitions are $(4.7 \pm 1.7) \times 10^{-3}$ and $(6.6 \pm 2.1) \times 10^{-3} \text{ M}_{\odot} \text{ yr}^{-1}$,

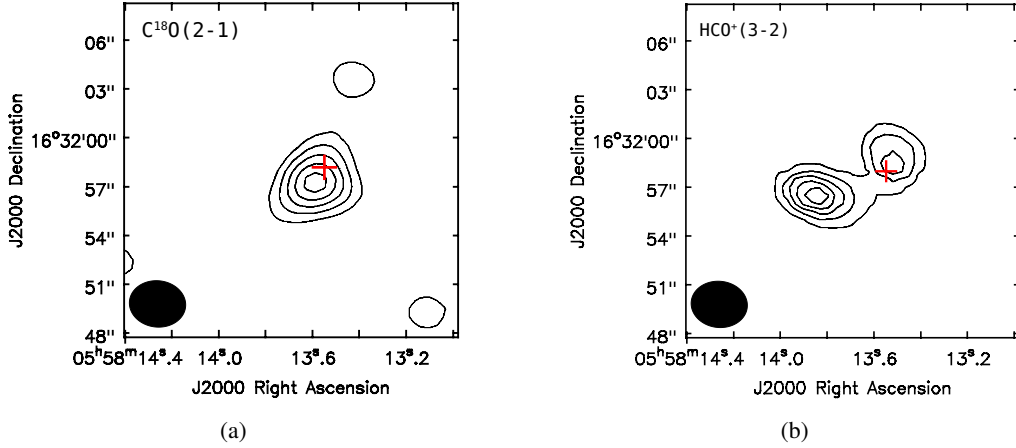


Fig. 4: Panels (a) and (b) present integrated intensity maps of $C^{18}O(2-1)$ and $HCO^+(3-2)$ transitions, respectively. The red cross of each panel is continuum emission peak of G192.16. The contour levels are from 10% to 90%, with step of 20%. The beam sizes of these two observations are shown in left-bottom corner of each panel. The $HCO^+(3-2)$ map is smoothed to same resolutions with $C^{18}O(2-1)$ map.

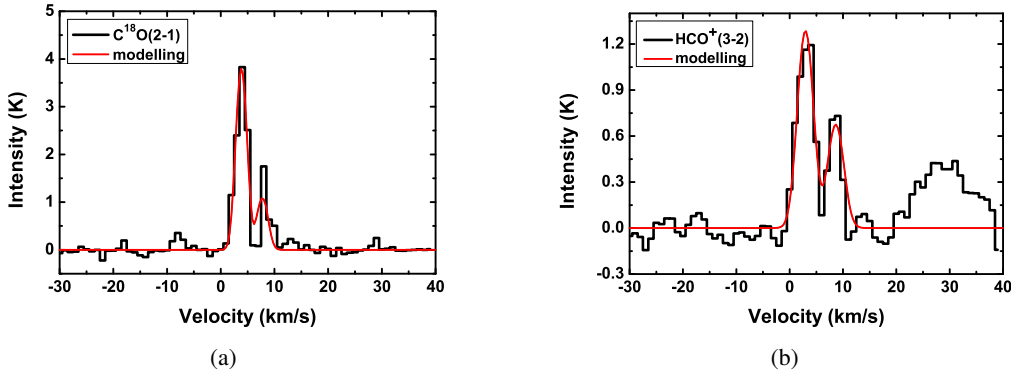


Fig. 5: Panels (a) and (b) present observed lines (black) and two-layer modelling (red) of $C^{18}O(2-1)$ and $HCO^+(3-2)$, respectively. The line name is shown in upper-left corner of each panel. The fitting results are listed in Table 3.

rates ranging from 10^{-4} to $10^{-2} M_{\odot} \text{ yr}^{-1}$ (Zhang & Ho 1997; Sandell et al. 2005; Beltrán et al. 2006; Garay et al. 2007; Zapata et al. 2008; Wu et al. 2009, 2014; Liu et al. 2011a,b, 2013a,b; Qin et al. 2016; Qiu et al. 2012). The derived infall rate toward G192.16 is consistent with those in other high-mass star formation regions.

In this work, infall rate of $C^{18}O(2-1)$ is $(4.7 \pm 1.7) \times 10^{-3} M_{\odot} \text{ yr}^{-1}$. $HCO^+(3-2)$ line has higher critical density than that of $C^{18}O(2-1)$, and it is generally used for tracing dense and inner parts of molecular clouds. Infall rate of $(6.6 \pm 2.1) \times 10^{-3} M_{\odot} \text{ yr}^{-1}$ is derived from $HCO^+(3-2)$, which is larger than that of $C^{18}O(2-1)$. The scenario appears to indicate that infall is faster in inner and denser region than in outer part of the G192.16 core. This is first time that infall motions have been reported in G192.16 massive core. The turbulent core model (Mckee & Tan 2003) considers a core having density structure of $\rho \propto r^{-1.5}$, the resulting accretion rate larger than $\sim 10^{-3} M_{\odot} \text{ yr}^{-1}$ will be high enough to overcome radiation pressure to form a massive star. In our case, the derived infall rate of $\sim 5 \times 10^{-3} M_{\odot} \text{ yr}^{-1}$ by assuming that the dense core

& Tan (2003). Recent numerical simulations have shown that massive star is formed by disk accretion, the radiation pressure barrier can be easily overcome when an optically thick accretion disk is taken into account (Kuiper et al. 2010; Kuiper & Yorke 2013). An accretion disk was also reported in G192.16, all these evidences indicate that a massive star is forming in G192.16 core by gas accretion, and high accretion rate is general requirement to form a massive star.

5 ACKNOWLEDGEMENTS

This work has been supported by the National Natural Science Foundation of China under grant Nos. 11373026 and 11433004, and the Joint Research Fund in Astronomy (U1631237) under cooperative agreement between the National Natural Science Foundation of China (NSFC) and Chinese Academy of Sciences (CAS), by Top Talents Program of Yunnan Province (2015HA030).

References

- Beltrán, M. T., Cesaroni, R., Codella, C., et al. 2006, *Nature*, 443, 427 8
- Beuther, H., Schilke, P., & Menten, K. M. 2002, *ApJ*, 566, 945 3, 5
- Di Francesco, J., Myers, P. C., Wilner, D. J., Ohashi, N., & Mardones, D. 2001, *ApJ*, 562, 770 5
- Fuller, G. A., Williams, S. J., & Sridharan, T. K. 2002, *AAS*, 200, 7115F 4
- Garay, G., Mardones, D., Bronfman, L., et al. 2007, *A&A*, 463, 217 8
- Hughes, V. A., & MacLeod, G. C. 1993, *AJ*, 105, 1495 2, 6
- Imai, H., Omodaka, T., Hirota, T., et al. 2006, *PASJ*, 58, 883 2, 6
- Jiang, Z., Tamura, M., Fukagawa, M., et al. 2005, *Nature*, 437, 112 1
- Kauffmann, J., Bertoldi, F., Bourke, T. L., Evens, II, N. J., & Lee, C. W. 2008, *A&A*, 487, 993 3
- Kuiper, R., Klahr, H., Beuther, H., & Henning, T. 2010, *ApJ*, 722, 1556 9
- Kuiper, R., & Yorke, H. W. 2013, *ApJ*, 763, 104 9
- Liu, T., Wu, Y., Zhang, Q., et al. 2011a, *ApJ*, 728, 91 4, 8
- Liu, T., Wu, Y., Liu, S.-Y., et al. 2011b, *ApJ*, 730, 102 4, 8
- Liu, T., Wu, Y., Zhang, H., 2013a, *ApJ*, 776, 29 4, 8
- Liu, T., Wu, Y., Wu, J., et al., 2013b, *MNRAS*, 436, 1335 4, 8
- Liu, H. B., Qiu, K., Zhang, Q., Girart, J. M., & Ho, P. T. P. 2013, *ApJ*, 771, 71 2, 3, 4, 6
- Liu, T., Li, P. S., Juvela, M., et al. 2018, *ApJ*, 859, 151 6
- Mckee, Christopher F., & Tan, Jonathan C. 2003, *ApJ*, 585, 850 8
- Myers, P. C., Mardones, D., Tafalla, M., et al. 1996, *ApJ*, 465, L133 5
- Patel, N. A., Curiel, S., Sridharan, T. K., et al. 2005, *Nature*, 437, 109 1
- Pineda, J. E., Maury, A. J., Fuller, G. A., et al. 2012, *A&A*, 544, L7 4, 6
- Qin, S. -L., Wang, J. -J., Zhao, G., Miller, M., & Zhao, J. -H. 2008, *A&A*, 484, 361 1
- Qin, S. -L., Schilke, P., Wu, J., et al. 2016, *MNRAS* 456, 2681 4, 8
- Qiu, K., Zhang, Q., Beuther, H., Fallscheer, C. 2012, *ApJ*, 756, 170 1, 4, 8

- Sault, R. J., Teuben, P. J., & Wright, M. C., 1995, in ASP Conf. Ser. 77, *Astronomical Data Analysis Software and systems IV*, ed. R. A. Shaw, H. E. Payne, & J. J. E. Hayes (San Francisco, CA: ASP), 433
2
- Shepherd, D. S., & Churchwell, E. 1996, *ApJ*, 472, 225 2
- Shepherd, D. S., Watson, A. M., Sargent, A. I., & Churchwell, E. 1998, *ApJ*, 507, 861 2, 3, 4, 5, 6
- Shepherd, D. S., & Kurtz, S. E. 1999, *ApJ*, 523, 690 2, 3, 6
- Shepherd, D. S., Claussen, M. J., & Kurtz, S. E. 2001, *Science*, 292, 1513 1, 2, 3, 5, 6
- Shepherd, D. S., Borders, T., Claussen, M. J., Shirley, Y. & Kurtz, S. E. 2004, *ApJ*, 614, 211 2, 6
- Shiozaki, S., Imai, H., Tafoya, D., et al. 2011, *PASJ*, 63, 1219 2, 3, 6
- Smith, R. J., Shetty, R., Stutz, A. M., & Klessen, R. S. 2012, *ApJ*, 750, 64 4
- Smith, R. J., Shetty, R., Beuther, H., et al. 2013, *ApJ*, 771, 24 4
- Sridharan, T. K., Williams, S. J., & Fuller, G. A. 2005, *ApJ*, 631, L73 1
- Sánchez-Monge, Á., Beltrán, M. T., Cesaroni, R., et al. 2014, *A&A*, 569, 11 1
- Williams, S. J., Fuller, G. A., & Sridharan, T. K. 2004, *A&A*, 417, 115 3, 5
- Wu, Jingwen., & Evans, Neal J., II. 2003, *ApJ*, 592, L79 4
- Wu, Y., Wei, Y., Zhao, M., et al. 2004, *A&A*, 426, 503 1
- Wu Y. F., Henke S., Xue R., Guan X., & Miller M. 2007, *ApJ*, 669, L37 4
- Wu, Y. F., Qin, S. -L., Guan, X., et al. 2009, *ApJ*, 697, L116 4, 8
- Wu, Y., Liu, T., & Qin, S. -L. 2014, *ApJ*, 791, 123 4, 8
- Zapata, L. A., Palau, A., Ho, P. T. P., et al. 2008, *A&A* 479, L25 4, 8
- Zhang, Q., & Ho, P. T. P. 1997, *ApJ*, 488, 241 8
- Zhang, Q., Hunter, T. R., & Sridharan, T. K. 1998, *ApJ*, 505, L151 1
- Zhou, S., Evans, N. J., II, Koempe, C., & Walmsley, C. M. 1993, *ApJ*, 404, 232 4